1-1-2018

Transcription factor Tbx18 induces the differentiation of c-kit^{+}canine mesenchymal stem cells (cMSCs) into SAN-like pacemaker cells in a co-culture model in vitro

Hua Xiao
The 452 Hospital of PLA, Third Military Medical University

Yong-Jun Yang
Third Military Medical University

Yi-Zhang Lin
Third Military Medical University

Song Peng
Third Military Medical University

Shu Lin
Third Military Medical University, University of Wollongong

See next page for additional authors

Transcription factor Tbx18 induces the differentiation of c-kit$^+$canine mesenchymal stem cells (cMSCs) into SAN-like pacemaker cells in a co-culture model in vitro

Abstract

Bone mesenchymal stem cells (MSCs), as well as cardiomyocytes, are derived from early mesoderm, becoming committed to their fate under the influence of different differentiation factors. We examined whether the overexpression of Tbx18 can induce the differentiation of c-kit$^+$ cMSCs into a phenotype similar to that of native pacemaker cells and whether these transfected cells can couple to adjacent atrial cells with functional consequences. The c-kit$^+$ cMSCs were first sorted, then transfected with different lentiviral vectors. Tbx18-c-kit$^+$ cMSCs represented the experimental group, while EYFP-c-kit$^+$ cMSCs and canine sinoatrial node (SAN) cells were used as controls. Within days of transfection, the hyperpolarization-activated cyclic nucleotide-gated (HCN) channel HCN4 protein and gap junction protein Connexin 45 (Cx45) expression in Tbx18-c-kit+cMSCs were 12-fold and 5.6-fold higher, respectively, than that in EYFP-c-kit$^+$ cMSCs. After co-culture with canine atrial cells in vitro for three days, the funny currents (If) were recorded in the Tbx18-c-kit$^+$ cMSCs, but not in EYFP-c-kit$^+$ cMSCs. The trend of these Ifcurrents was highly similar to that of SAN cells, although the current density was smaller. The Tbx18-EYFP-c-kit$^+$ cMSCs showed responsiveness to β-adrenergic stimulation, and the intracellular cyclic adenosine monophosphate (cAMP) level was higher than that in EYFP-c-kit$^+$ cMSCs. The Tbx18-EYFP-c-kit$^+$ cMSCs delivered fluorescent dye to neighboring atrial cells via gap junctions, thus these cell pairs could communicate as a pacemaker unit. We propose that the overexpression of Tbx18 in c-kit$^+$ cMSCs induces their differentiation to SAN-like pacemaker cells.

Disciplines

Medicine and Health Sciences

Publication Details

Xiao, H., Yang, Y., Lin, Y., Peng, S., Lin, S. & Song, Z. (2018). Transcription factor Tbx18 induces the differentiation of c-kit$^+$canine mesenchymal stem cells (cMSCs) into SAN-like pacemaker cells in a co-culture model in vitro. American Journal of Translational Research, 10 (8), 2511-2528.

Authors

Hua Xiao, Yong-Jun Yang, Yi-Zhang Lin, Song Peng, Shu Lin, and Zhi-Yuan Song

Am J Transl Res 2018;10(8):2511-2528
www.ajtr.org /ISSN:1943-8141/AJTR0077938

Original Article

Transcription factor Tbx18 induces the differentiation of c-kit$^+$ canine mesenchymal stem cells (cMSCs) into SAN-like pacemaker cells in a co-culture model in vitro

Hua Xiao[1,2], Yong-Jun Yang[1], Yi-Zhang Lin[1], Song Peng[1], Shu Lin[1,3], Zhi-Yuan Song[1]

[1]Department of Cardiology, Southwest Hospital, Third Military Medical University (Army Medical University), Chongqing 400038, P.R. China; [2]Department of Cardiology, The 452 Hospital of PLA, Chengdu 610000, Sichuan, P.R. China; [3]School of Medicine, University of Wollongong and Illawarra Health and Medical Research Institute, NSW 2522, Australia

Received April 15, 2018; Accepted July 8, 2018; Epub August 15, 2018; Published August 30, 2018

Abstract: Bone mesenchymal stem cells (MSCs), as well as cardiomyocytes, are derived from early mesoderm, becoming committed to their fate under the influence of different differentiation factors. We examined whether the overexpression of Tbx18 can induce the differentiation of c-kit$^+$ cMSCs into a phenotype similar to that of native pacemaker cells and whether these transfected cells can couple to adjacent atrial cells with functional consequences. The c-kit$^+$ cMSCs were first sorted, then transfected with different lentiviral vectors. Tbx18-c-kit$^+$ cMSCs represented the experimental group, while EYFP-c-kit$^+$ cMSCs and canine sinoatrial node (SAN) cells were used as controls. Within days of transfection, the hyperpolarization-activated cyclic nucleotide-gated (HCN) channel HCN4 protein and gap junction protein Connexin 45 (Cx45) expression in Tbx18-c-kit$^+$ cMSCs were 12-fold and 5.6-fold higher, respectively, than that in EYFP-c-kit$^+$ cMSCs. After co-culture with canine atrial cells in vitro for three days, the funny currents (I_f) were recorded in the Tbx18-c-kit$^+$ cMSCs, but not in EYFP-c-kit$^+$ cMSCs. The trend of these I_f currents was highly similar to that of SAN cells, although the current density was smaller. The Tbx18-EYFP-c-kit$^+$ cMSCs showed responsiveness to β-adrenergic stimulation, and the intracellular cyclic adenosine monophosphate (cAMP) level was higher than that in EYFP-c-kit$^+$ cMSCs. The Tbx18-EYFP-c-kit$^+$ cMSCs delivered fluorescent dye to neighboring atrial cells via gap junctions, thus these cell pairs could communicate as a pacemaker unit. We propose that the overexpression of Tbx18 in c-kit$^+$ cMSCs induces their differentiation to SAN-like pacemaker cells.

Keywords: Tbx18, c-kit$^+$ mesenchymal stem cells, HCN4, gap junction, co-culture

Introduction

Bioengineered cell therapy is an alternative to electronic pacemakers; since regular testing and replacement are not needed, there are no lethal complications or electromagnetic interference risks, and the method is suitable for low weight children. The most attractive benefit of this therapy is physiological autonomic responsiveness [1]. The bioengineered pacemaker itself does not necessarily an excitable cell and shouldn't have the overall ion channels of the native sinoatrial node cell. The bioengineered pacemaker act as a donor, automaticity delivering the lacking element of the working myocardium to contiguous excited cells via gap junctions. This pattern forms a functional syncytium to yield sustained pacing. As the ideal stem cells for biological pacemaker therapy, bone marrow-derived mesenchymal stromal stemcells (MSCs) have the advantage of immune privilege, are electrically quiescent and express two cardiac gap junctional proteins, Cx40 and Cx43 [2, 3]. The current approach focuses on I_f overexpressing MSCs to create a biological pacemaker because I_f rapidly deactivates upon depolarization and does not impact the action potential duration. MSCs have the potential to directly differentiate into cardiomyocytes, but this cardiac cellular phenotype differentiation potential is weak [4, 5]. In addition, some groups explored autologous SAN cell transplantation, but failed to provide sustained biological pacemaker activity, emphasizing the

critical role of the substrate [6, 7]. In previous studies, we demonstrated that mHCN4-infected cMSCs can generate a functional I_f current. However, when delivering the biological pacemaker to the canine heart, the spontaneous rates did not satisfy the demand of normal physiological activity (45±9 beats/min) [8, 9]. We hypothesize that the cause of this phenomenon maybe the loss of HCN4 after engrafting in vivo and the inappropriate connexin coexpression ratio between the HCN4-transfected cells and a quiescent myocyte [10].

Myocardial regeneration by direct injection of c-kit+ bone marrow stem cells in a mouse model was first reported by Orlic and colleagues in 2001 [11]. By using viral gene-tagging, multicolor clonal-marking and transcriptional profiling methods, Anna et al. demonstrated that single mouse c-kit-bone marrow cells (BMCs) clonally expanded within the infarcted myocardium and differentiated into specialized cardiac cells. Newly formed cardiomyocytes, endothelial cells, fibroblasts and c-kit-BMCs had common sites of viral integration in their genomes, strongly supporting the plasticity of a subset of BMCs expressing the c-kit receptor. The bone marrow comprises a category of cardiomyogenic, vasculogenic and/or fibrogenic c-kit+ cells and a category of c-kit+ cells that retains an undifferentiated state [12]. Freshly isolated c-kit+Lin- cells from rat hearts generated the major specialized cell types of the heart: myocytes and vascular cells, suggesting that c-kit is a marker of cardiac stem cells and maybe the earliest marker of the cardiomyocyte *lineage* differentiation of stem cells [13, 14]. Taken together, c-kit+-MSCs could be used for heart regeneration therapy because of their high potential for cardiomyocyte and endothelial differentiation. The T-box gene family proteins are the main regulators of myocardial proliferation and patterning. Transcriptional regulators, such asTbx3, Tbx5, and Tbx18, play critical roles in embryonic sinoatrial node (SAN) development [15]. Upstream of these factors is Tbx18, which is a member of the Tbx1 subfamily, associated with the cardiac venous pole that contributes to the outer tissue layer of the heart, the cardiac pacemaker, as well as the myocardium of the sinus venosus region. From embryonic day (E) 9.5 to E 14.5, the sinus venosus mesenchymal progenitor cells expressing Tbx18 define the sinus venosus and differentiate into the myocardium of the head region of the SAN. The border between SAN and the atrial myocardium of a Tbx18 null allele homozygous mice is vague, and these mice have dramatically reduced SAN areas [16, 17]. Therefore, we hypothesized that the overexpression of Tbx18 could induce c-kit+ cMSCs to become SAN-like pacemaker (iSAN) cells. In the present study, we examined the use of a cell-based approach to construct an ideal biological pacemaker with robust and sustaining pacing capability and a sensitive response to autonomic-nerve modulation that resembles a native pacemaker. Additionally, this biological pacemaker can communicate with the coupled cardiac cells via gap junctions under optimal co-culture conditions. We aimed to achieve two goals: 1) improve pacemaker function by the overexpression of Tbx18 in canine c-kit+-cMSCs to induce a phenotype similar to that of native pacemaker cells; and 2) couple Tbx18-transfected c-kit+-cMSCs with canine atrial cells to create a functional two-cell syncytium.

Materials and methods

Ethics statement

The protocols of the present study were performed in accordance with the Guide for the Care and Use of Laboratory Animals to minimize animal suffering and approved by the ethics committee of Animal Experiments of the Third Military Medical University (Permit Number: SYXK2012-0031).

Sorting of c-kit+ cMSCs

Canine mesenchymal stem cells (cMSCs) were isolated from the bone marrow of five dogs (either sex; ages ranging from neonate to one month, Third Military Medical University, Chongqing, China), weighing 0.3-2.5 kg, as previously described [18]. Briefly, bone marrow aspiration from the femurs and tibias was performed on dogs anesthetized with 30-mg/kg intravenous sodium pentobarbital (Sigma-Aldrich, St. Louis, MO, USA). The obtained cells were cultivated in Dulbecco's Modified Eagle Medium (DMEM, Gibco; Thermo Fisher Scientific, Inc., Waltham, MA, USA), supplemented with 10% fetal bovine serum (FBS, Gibco; Thermo Fisher Scientific, Inc., Waltham, MA, USA), 100 U/ml penicillin and 100 μg/ml streptomycin (Beyotime Institute of Biotechnology,

China), seeded onto 6-well plates (NEST, Biotechnology Co., Ltd.) and incubated in a 37°C, 5% CO_2-humidified atmosphere. The medium was changed every 2 days to wash out nonadherent hematopoietic cells.

Using trypan blue exclusion, the third passage cells were first used for flow cytometric live cell sorting. Briefly, these cells were suspended in phosphate-buffered saline (PBS, ZSGB Biotech Co., Ltd., Beijing, China) containing 2% FBS to obtain a density of 8×10^6 cells per milliliter, then incubated in the dark for approximately 60 min at room temperature with a PE/Cy5-conjugated antibody against c-Kit (Abcam; ab157301; 1:50) and analyzed by using a flow cytometer with 561 nm excitation. Cy5 fluorescence emission was detected with a 670/30 bandpass filter. The gates were drawn with unstained cells. Sorting was performed at low influx pressure (20 psi) by using a 100-μm nozzle. The number of c-kit+ cMSCs equals the total number of tested cells within a gate multiplied by the percentage (× %) of c-kit positive cells. The cells under post-sort analysis typically indicated a purity of > 90%, with minimal cell death (< 10%). The abovementioned operating procedures were sterile, and the sorted c-kit+ cMSCs were centrifuged (300 g for 5 min) and resuspended in DMEM containing 20% FBS, 100 U/ml penicillin and 100 μg/ml streptomycin. Part of these cells was then identified via flow cytometric analysis with $CD45^-/CD29^+/CD44^+$ [8]. The remaining cells were subcultured for the following experiment. Flow cytometric analysis and sorting were performed by using the BD Influx Flow Cytometer, which included a software package to analyze the data (BD Biosciences, San Jose, CA, USA).

Construction of hTbx18 lentiviral vector and hTbx18 infection

The lentiviral vector expressing hTbx18, pLV[Exp]-Puro-EF1A > hTBX18[NM_001080508.2]:T2A:{EYFP} (~11.1 kb) was constructed by Gateway recombination cloning using Gateway-adapted vectors (Cyagen Biosciences Inc., Guangzhou, China). The LR (Entry Clones attL × Target Vectors attR) recombination reaction was performed between the entry clone and the destination vector. This reaction system included the plasmid pUp-EF1A (12.89 ng), pDown-hTBX18 (10.42 ng), pTail-T2A:EYFP (13.03 ng) and the vector backbone pLV.Des3d.P/puro (60.28 ng), in which gene expression is controlled by the EF1A promoter and the expression of Tbx18 is linked to enhanced yellow fluorescent protein (EYFP) expression. Positive constructs were verified to have the correct target gene by PCR, DNA sequencing and restriction enzyme digestion. The lentiviral vector pLV[Exp]-Puro-EF1A > {EYFP} (~9.2 kb) was constructed as a control group. Lentiviral particles were prepared by cotransfecting the transfer plasmid, packaging plasmids and envelope plasmid into 293T cells in a 10-cm dish. The supernatant-containing virus was collected and centrifuged at 50,000 g for 2 h. The precipitate was resuspended in an appropriate volume of PBS and stored at -80°C.

The c-kit+ cMSCs were transfected with pLV-hTbx18-EYFP or pLV-EYFP in the presence of 5 μg/ml of polybrene (Sigma-Aldrich) at a multiplicity of infection (MOI) of 100 for 24 h. The expression of EYFP after 48 h was > 90% for both types of infected cells, which were analyzed by confocal laser microscope images in at least four different random fields.

Preparation of canine SAN cells

Single SAN cells were isolated from canine hearts based on a previous method used for mice [19]. Briefly, ten one-month-old dogs (either sex; 1.5 to 2.5 kg; Third Military Medical University, Chongqing, China) were included. The dogs were intravenously injected with a euthanasia dose of sodium pentobarbitone (100 mg/kg). After the loss of consciousness and withdrawal reflexes, the hearts were quickly excised and placed in cold Tyrode solution, comprising (mM) 140 NaCl, 5.0 HEPES, 5.5 glucose, 5.4 KCl, 1.8 $CaCl_2$ and 1.0 $MgCl_2$, pH adjusted to 7.4 with NaOH. The canine sinoatrial node region, identified as a whitish endocardial zone near the junction between the superior vena cava and the RA appendage was dissected from the heart under the microscope, then cut into small chunks, during which spontaneous activities were observed [20]. The small chunks were rinsed in a "low Ca^{2+}" solution containing (mM) 140 NaCl, 5.0 HEPES, 5.5 glucose, 5.4 KCl, 0.2 $CaCl_2$, 0.5 $MgCl_2$, 1.2 KH_2PO_4, 50 taurine and 1 mg/ml bovine serum albumin (BSA, Gibco; Thermo Fisher Scientific, Inc., Waltham, MA, USA), with pH adjusted to 6.9 with NaOH, digested in 10 ml of enzyme solution with type I collagenase (Sigma-Aldrich),

Table 1. Primers used in reverse transcription-quantitative polymerase chain reaction analyses

Gene	Forward	Reverse
Cx43	5'-CACTGAGCCCCTCCAAAGAC-3'	5'-TTGCTCACTTGCTTGTTTGTTG-3'
Cx45	5'-GCAGAACCAACCTAAACCCAAG-3'	5'-TGCCCTATCAGAAAACCCACC-3'
Kir2.1	5'-TGGGAACGGGAAGAGTAAGG-3'	5'-ACGAACGCCAGGCAGAAG-3'
Nav1.5	5'-GCATGGCTAACTTCGCTTATG-3'	5'-AGGATGGGGCTGAGGAGG-3'
PLB	5'-GTCCAATACCTCACTCGCTCTG-3'	5'-CAATGATGCAGATCAACAAGAGAC-3'
α-actinin	5'-AGCCACCTGCGACAGTACG-3'	5'-CTGGCGATGGTGGTGAGG-3'
Nkx2-5	5'-AGAAAGAGCTGTGCTCACTGC-3'	5'-CTCAGGGGCCGACAGATAC-3'
β-actin	5'-GCCCATCTATGAGGGGTACG-3'	5'-TGATGTCACGCACGATTTCC-3'

Cx43, Connexin 43; Cx45, connexin 45; Kir2.1, the strongest inward rectifying K^+ channel; Nav1.5, tetrodotoxin-resistant voltage-gated sodium channel; PLB, phospholamban.

elastase (Sigma-Aldrich), and protease type XIV (Sigma-Aldrich). The digestion was performed for approximately 20 min at 35°C, under manual mechanical agitation. The tissue was subsequently transferred into Kraft-Brule medium containing (mM) 100 potassium glutamate, 5.0 HEPES, 20 glucose, 25 KCl, 10 potassium aspartate, 2.0 $MgSO_4$, 10 KH_2PO_4, 20 taurine, 5 creatine, 0.5 EGTA, and 1 mg/ml BSA, with pH adjusted to 7.2 with KOH, where the cells were separated and then stored at 4°C until further use. All freshly isolated cells were used for experiments within 6 hours after isolation.

RT-PCR and RT-qPCR test

Tbx18-EYFP and EYFP-transfected c-kit+ cMSCs (4 days post transfection) were respectively collected, and total RNA was extracted from these cells by using Beyozol (Beyotime Institute of Biotechnology, R0011, Shanghai, China). The mRNA sample was converted to first-strand cDNA by using the PrimeScript™ II 1st strand cDNA Synthesis Kit (Takara 6210A/B). NCBI database provided the CDS of TBX18 (Gene ID:9096), Primer-BLAST designed Primer sequence: TBX18-homo-F: 5'-ACGTCATCCGTAAAGACTGTGG-3', TBX18-homo-R: 5'-AGTCCGTAGTGATGGTCGCC-3', the cDNA template was mixed with Premix Taq™ (Ex Taq™, Version 2.0, Takara RR902Q), gene-specific primer sets and DNase/RNase-free water. The PCR was performed on the CFX96™ System (Bio-Rad, USA). The resulting products were separated by electrophoresis on a 1%-(w/v)-agarose gel in TAE, and the relative expression of the gene was 251 bp.

RT-qPCR was performed according to a previous study [21]. All primers (**Table 1**) were synthesized by Invitrogen, Thermo Fisher Scientific, Inc. (Shanghai, China). The total cellular mRNA of Tbx18-EYFP, EYFP-transfected c-kit+ cMSCs and canine SAN cells was respectively extracted by using TRIzol (Beyotime Institute of Biotechnology, China). Subsequently, the cDNA synthesis was performed according to the manufacturer's instructions. RT-qPCR was performed with SYBR Green Real-time PCR Master mix (QPK-201, Toyobo, Co., Ltd., Osaka, Japan) on a CFX96™ Real-Time PCR System (Bio-Rad, USA). The relative changes were normalized to β-actin mRNA by using the $2^{(-\Delta\Delta Ct)}$ method. All results were repeated three times.

Immunofluorescence and immunoblotting

The c-kit+ cMSCs, Tbx18-EYFP-c-kit+ cMSCs, EYFP-c-kit+ cMSCs, and canine SAN cells were respectively fixed with 4% paraformaldehyde (Sangon Biotech Co., Ltd., Shanghai, China) for 15 min at room temperature, washed in PBS, blocked with 6% normal goat serum (HyClone, GE Healthcare Life Sciences, USA) in PBS for 30 min at room temperature. These cells were first permeabilized with 0.2% Triton X-100 (Sangon Biotech Co., Ltd., Shanghai, China) for 15 min and subsequently nonspecific binding was blocked, followed by incubation with anti-Cx45 (Abcam; ab78408; 1:100) at 4°C overnight to detect the expression of certain proteins in the cytoplasm. Subsequently, these cells were washed three times with PBS and then incubated in the dark with goat anti-mouse IgG labeled with cy3 (Abcam, ab97035, 1:800) at 37°C for 30 min. After further washing, these cells were counter-stained with DAPI (Beyotime Institute of Biotechnology, C1002, 1:1000) for 5 min prior to mounting (Antifade mounting medium, Beyotime Institute of Biotechnology,

Shanghai, China). Imaging was performed on a Zeiss LSM710 laser confocal microscope (Carl Zeiss Microscopy GmbH, Jena, Germany). ZEN lite 2011 software (Carl Zeiss Microscopy GmbH) was used to analyze the data. Western blotting was performed by using specific antibodies against Cx43 (Abcam, ab11370; 1:1000), Cx45 (Abcam; ab78408; 1:1000), sarcomeric α-actinin (Sigma-Aldrich; A5044; 1:500), PLB (Abcam, ab2865; 1:1000), p-PLB (Abcam, ab15000; 1:1000), and HCN4 (AbCam; ab85023; 1:1000). Briefly, Tbx18-c-kit+ cMSCs, EYFP-c-kit+ cMSCs and canine SAN cells were respectively lysed in radioimmunoprecipitation assay buffer containing phenylmethylsulfonyl fluoride (RIPA) buffer and the protease inhibitor (PMSF). Protein content was quantified by BCA assay, and the cell lysates (200 μg per lane for sarcomeric α-actinin, 80 μg per lane for the others) were run on a 10% (HCN4 and sarcomeric α-actinin) or 12% (Cx45, Cx43, PLB, and p-PLB) SDS-PAGE gel and transferred onto a PVDF membrane. Then, the transferred membrane was incubated with a primary antibody overnight at 4°C, followed by 1-hour incubation with a peroxidase-conjugated secondary antibody. Immunoreactivity was detected by chemiluminescence (ECL Western Blotting Analysis System, Amersham). Equal protein loading of the gels was assessed by reprobing the membrane with monoclonal anti-GAPDH antibody (Abcam; ab9482; 1:10000). The experiments were performed several times to verify the results.

cAMP assay

Canine cAMP ELISA Kit (JL16767-48T; J&L Biological) was used to determine cAMP levels in canine SAN cells and c-kit+ cMSCs transduced with pLV-hTbx18-EYFP or pLV-EYFP. Briefly, 50 μl of the lysates from the three groups and standards (standard concentration was followed by 20, 10, 5, 2.5, 1.25, 0.625 nmol/l) were respectively added to the appropriate wells of a microtiter plate. Then, 100 μL of Enzyme conjugate was added to each tested well, which covered with an adhesive strip, and incubated for 60 minutes at 37°C. After washing, 100 μL of chemiluminescent reagent was added to each well and incubated in the dark for 15 minutes at 37°C. After adding 50 μL of stop solution to each well, the intensity of the color was measured at 450 nm by using a microplate reader (Varioskan Flash, Thermo Scientific). The concentration of cAMP in the three tested groups was determined by comparing the optical density of the tested group to that of the standard curve.

Preparation of canine atrial cells and co-culture conditions

The right atriums were removed from the hearts of abovementioned neonatal dogs, cut into small strips and washed with Tyrode solution to remove the blood. Then, digested in 10 ml of enzyme solution with type I collagenase (Sigma-Aldrich) and trypsin (Ameresco, Solon, OH, USA) in Ca^{2+} Mg^{+}-free D-Hanks (Wuhan Boster Biological Technology, Ltd., Wuhan, China) for approximately 30 min. The isolated cells were preplated to reduce the fibroblast contamination. Only cells with a rod-shaped appearance were used in the present study. For co-culture experiments, Tbx18-c-kit+ cMSCs or EYFP-c-kit+ cMSCs were mixed with atrial cells and plated at a ratio of 1:4 (20% c-kit+ cMSCs) onto the twelve confocal dishes (NEST, Biotechnology Co., Ltd.). The cell mixtures were co-cultured for three days as isotropic monolayers, with the medium changed every two days. Fluorescence mapping was performed after three days in culture, and Tbx18-c-kit+ cMSCs or EYFP-c-kit+ cMSCs were identified with yellow fluorescence observed by using the Zeiss LSM710 laser confocal microscope (Carl Zeiss Microscopy GmbH, Jena, Germany). The co-culture experiment was performed three times to validate the results.

Electrophysiological measurements

For electrophysiological recordings, glass coverslips with adherent cells were transferred to an experimental chamber mounted on the stage of an inverted microscope (OLYMPUS, LUMPlanFI/IR), equipped with a fluorescence imaging system. The chamber was perfused at 36±1°C with normal Tyrode solution by using a gravitational perfusion system. The data were recorded with the Axonpatch 200B amplifier (Axon Instruments, Foster City, CA, USA) under the control of the pCLAMP 10.1 software (Axon Instruments). Membrane currents were filtered at 5 kHz and digitized at a sampling rate of 10 kHz. The membrane capacity was measured by application of a voltage clamp step, and current densities were expressed as the value of the peak current per capacity. Canine SAN cells were easily identified prior to voltage clamp

studies by their typical morphology (spindle or spider shape), sustained rhythmic activity, and smaller size compared to atrial myocytes. Perforated (amphotericin B, 250 g/ml) whole-cell patch-clamp and voltage-clamp techniques were used to record membrane ion channel currents of SAN. The whole-cell patch clamp technique was used to study membrane currents in Tbx18-c-kit+ cMSCs and EYFP-c-kit+ cMSCs. I_f was recorded as previously described [20, 22]. The currents were elicited with the command voltage steps ranging from -40 mV to -160 mV in -10 mV increments followed by a step to +20 mV from the holding potential of -30 mV. The patch pipettes had a resistance of 4-6 MΩ (SAN) or 3-5 MΩ (cMSCs), which were filled with intracellular solution, containing (mmol/l): 120 potassium aspartate, 25 KCl, 4.0 $MgCl_2$, 10 EGTA, 4.0 KATP, 2.0 NaGTP, 2.0 phosphocreatine, 5.0 HEPES, 1.0 $CaCl_2$, and pH was adjusted to 7.2 with KOH. The extracellular solution contained (mmol/l): 130 NaCl, 5.0 KCl, 2.0 $MgCl_2$, 1.8 $CaCl_2$, 5.0 HEPES, and the pH was adjusted to 7.4 with NaOH. The I_f current was routinely recorded in Tyrode solution containing 1 mmol/l $BaCl_2$ to eliminate the Ba^{2+}-sensitive component of K^+ current, 10 mmol/l 4-AP, and 10 mmol/l TTX were also added when measuring the I_f reversal potential and fully activated current-to-voltage relation [23]. After the I_f was recorded, the cells were superfused with an extracellular solution containing 5-mmol/l cesium chloride, and the currents were measured accordingly. Tail currents were measured immediately after the step to +20 mV. The membrane potential of half-maximal activation ($V_{1/2}$) and the slope factor (k) were obtained by fitting the activation curves to the Boltzmann equation $I_{tail}/I_{max} = A/\{1 + \exp[(V-V_{1/2})/K]\}$. The time constants of activation were determined by fitting current traces to a single exponential function. The activation voltage protocol was applied for 4 s when 3 μmol/l isoproterenol was added to the extracellular solution to study I_f activation kinetics. To determine the reversal potential and the deactivation time constants of I_f, the voltage protocol was to hold the voltage at -30 mV and hyperpolarize the cells to -150 mV, followed by a depolarization to voltages between -150 and +20 mV for 2 s to record the tail currents necessary to construct the fully activated current-voltage relation, and a subsequent step to -10 mV. The time course of I_f deactivation was fitted by the monoexponential equation $I_{tail}/I_{max} = A \times [1-\exp(-t/\tau)]$ [24]. All chemicals mentioned above were obtained from Sigma (St Quentin, Fallavier). Intercellular communication via gap-junctions was determined by using Lucifer yellow dye (Sigma Aldrich, St Louis, MO, USA) among the three groups: 1. a pair of SAN cells, 2. Tbx18-c-kit+ cMSCs and canine atrial cells, 3. EYFP-c-kit+ cMSCs and canine atrial cells. Briefly, on the basis of perforated whole-cell patch clamp (group 1) or whole-cell patch clamp (group 2 and 3) recording, the 0.1% Lucifer yellow dye pre-incorporated into the internal solution was loaded into a SAN cell or target cell, which was identified by one cell of the pair expressing I_f currents and EYFP (group 2) or EYFP alone (group 3), and the number of coupled cells was determined after a 5-min dye transfer.

Statistics

The data are presented as the means ± standard error of the mean (SEM) and were analyzed by using SPSS (version 25; SPSS Inc., Chicago, IL, USA). Statistical comparisons among multiple groups were estimated by one-way analysis of variance with Dunnett's T3 test. Curve fitting was performed by using Origin (version 9.1; Originlab Corp., Northampton, USA). Values of $P < 0.05$ were considered statistically significant.

Results

Representative flow cytometry method for c-kit+ cMSCs sorting and identification

First, flow cytometric live cell sorting was used to separate c-kit+ from c-kit- cells. Sorting setup and appropriate gating were established, and post-sort analysis indicated a purity of c-kit+ cells > 90% with minimal cell death (< 10%, **Figure 1A**, **1B**). The cMSCs have chondrogenic, osteogenic and adipogenic lineages differentiation ability, expression of CD29, CD44 and absence of hematopoietic (stem) cell markers CD34, CD45 and CD133 [8]. Flow cytometry analysis of the gated c-kit+ cells showed the characteristic of MSCs (**Figure 1C-E**).

Demonstration of gene transfer

At 48 hours after transfection, the infected cMSCs exhibited yellow fluorescence. The transfection rates of pLV-hTbx18-EYFP-c-kit+

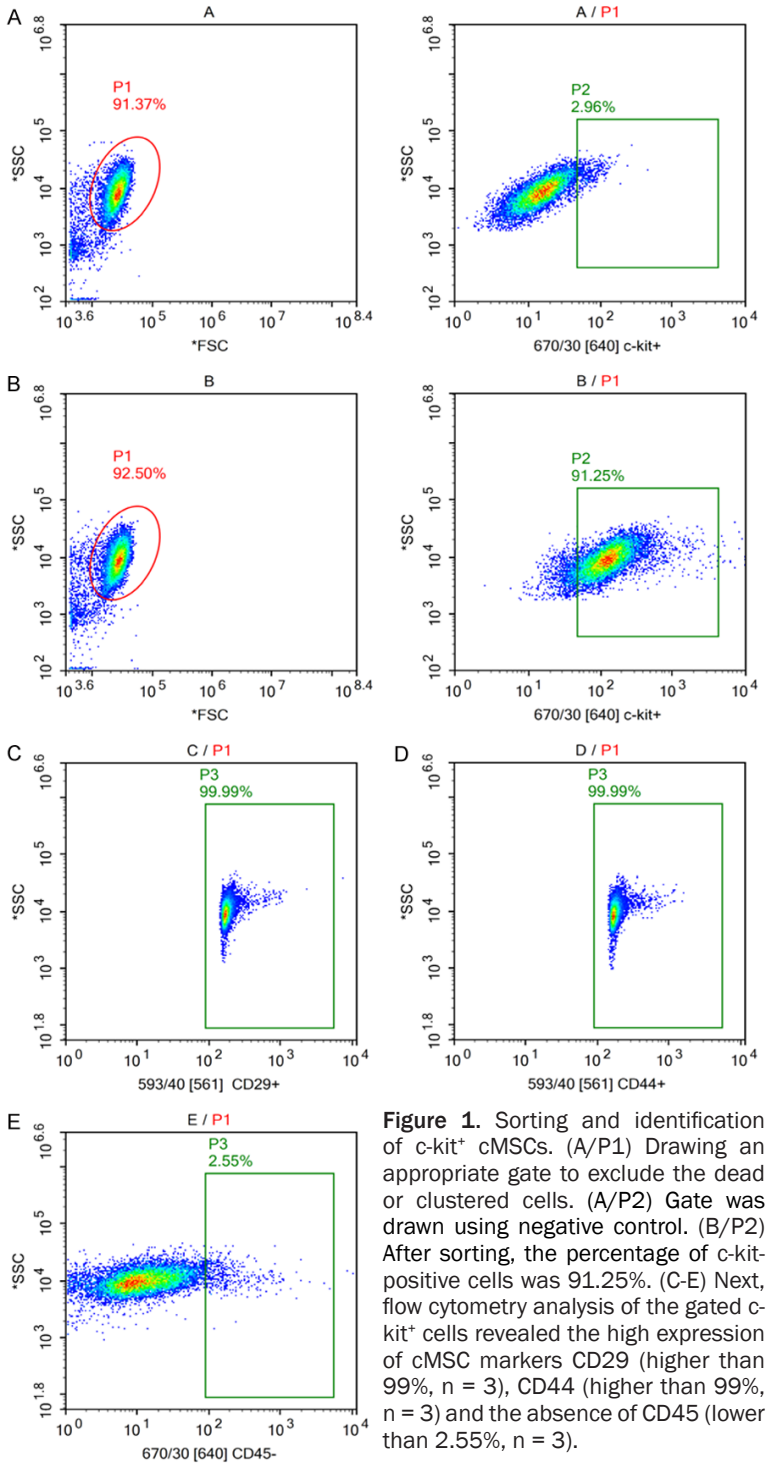

Figure 1. Sorting and identification of c-kit+ cMSCs. (A/P1) Drawing an appropriate gate to exclude the dead or clustered cells. (A/P2) Gate was drawn using negative control. (B/P2) After sorting, the percentage of c-kit-positive cells was 91.25%. (C-E) Next, flow cytometry analysis of the gated c-kit+ cells revealed the high expression of cMSC markers CD29 (higher than 99%, n = 3), CD44 (higher than 99%, n = 3) and the absence of CD45 (lower than 2.55%, n = 3).

cMSCs and pLV-EYFP-c-kit+ cMSCs were 94±3.5% and 96±2.5% respectively, which were analyzed by laser confocal microscopy in six different random fields (**Figure 2A**, **2B**, magnification of the final image, × 200, scale bar = 75 μm). RT-PCR analysis confirmed the designed TBX18 primer based on detection of the TBX18 gene in Tbx18-c-kit+ cMSCs.

Electrophysiological effects of Tbx18 overexpression in c-kit+ cMSCs under co-culture conditions

After co-culture with canine atrial cells for three days, the electrophysiological characteristics were tested. I_f currents were evaluated in Tbx-18 overexpression after-sorting c-kit+ cMSCs, which were compared with SAN cells by using the whole-cell patch-clamp technique. EYFP-c-kit+ cMSCs served as a control. From a holding potential of -30 mV to voltages ranging from -40 to -160 mV in -10 mV increments (**Figure 3A**), Tbx18-c-kit+ cMSCs elicited time and voltage dependent hyperpolarization-activated inward currents which reversible blocked by Cs^+, a specific I_f blocker (**Figure 3B**). No typical I_f currents were recorded from EYFP-c-kit+ cMSCs (**Figure 3C**). Current-voltage (I-V) relationships of I_f (**Figure 3D**) showed that the current density of Tbx18-c-kit+ cMSCs and SAN cells was 5.7±0.3 pA/pF (n = 22) and 7.5±0.3 pA/pF (n = 18) at -120 mV, and 7.6±0.1 pA/pF (n = 22) and 9.4±0.1 pA/pF (n = 18) at -160 mV. Differences in the current density at same voltage reached statistical significance ($P < 0.05$ for each). The data of these different cells showed lower values than those reported for SAN cells from small animals, such as rabbits (10±4.8 pA/pF) [25] and mice (18±2 pA/pF) [26]. Similar to the currents measured in isolated human SAN cells (~6 pA/pF) [27], the relatively lower I_f density contributes to the slower heart rate which is the characteristic of large ani-

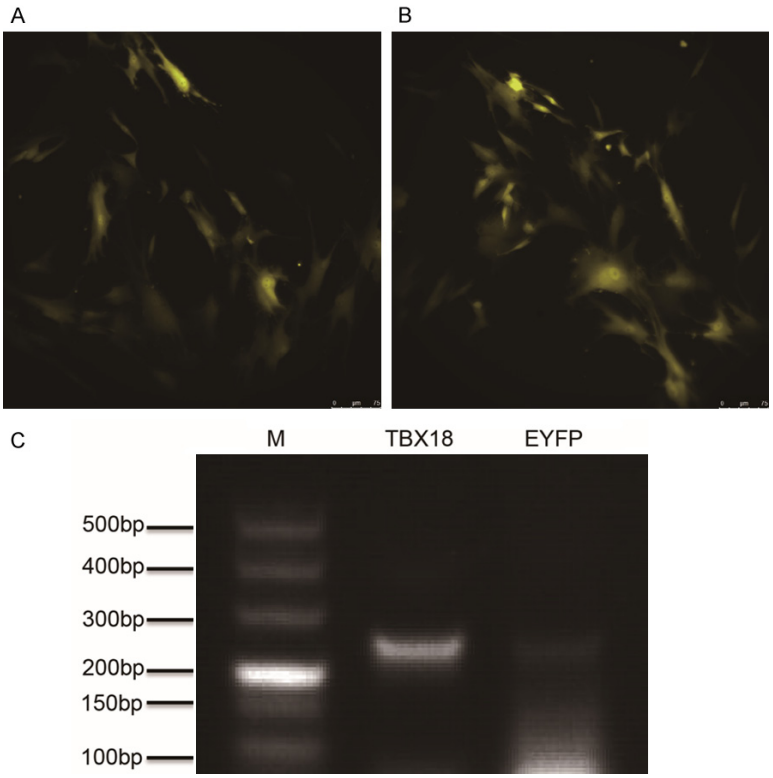

Figure 2. Verification of hTbx18 overexpression in Tbx18-EYFP-c-kit+ cMSCs. Laser confocal microscopy of c-kit+ cMSCs after transfection. The c-kit+ cMSCs were transfected with pLV-hTbx18-EYFP (A) and pLV-EYFP (B), as evidenced by the expression of yellow fluorescence. Scale bar: 75 μm. (C) Reverse transcription (RT)-polymerase chain reaction (PCR) further confirmed hTbx18 overexpression in Tbx18-EYFP-c-kit+ cMSCs. EYFP-c-kit+ cMSCs were used as a control. Lane M is a DL 500 ladder marker. The length of the amplicons for lane Tbx18 was 251 bps.

mals. Tbx18-EYFP-c-kit+ cMSCs laid the foundation for future use of large animals in vivo research. We further constructed regression models by using I_f currents (I) and testing voltage (V). The trend of typical I_f currents in Tbx18-EYFP-c-kit+ cMSCs and SAN was highly similar, which reached statistical significance ($I = -89.368 + 82.306\ V - 19.975\ V^2 + 0.868\ V^3$, $F = 693.056$, Sig. < 0.01, $R^2 = 0.983$ vs. $I = -110.892 + 102.927\ V - 26.637\ V^2 + 1.204\ V^3$, $F = 649.977$, Sig. < 0.01, $R^2 = 0.982$). The activation characteristic of the I_f voltage-gated channel was evaluated from tail currents, which were normalized to the maximum value, plotted as the reaction of preceding hyperpolarizing potential, and fit with a Boltzmann equation to gain the midpoint activation voltage ($V_{1/2}$) and slope factor (k) for Tbx18-EYFP-c-kit+ cMSCs and SAN cells (**Figure 3E**). The differences of $V_{1/2}$ between these two types of cells reached statistical significance (-82.5±4.6, n = 22 vs. -77.2±6.3 mV, n = 18; P < 0.05), but the k did not (-7.7±0.4, n = 22 vs. -8.1±0.2 mV, n = 18; P = 0.573). The voltage dependences of the fully activated currents were assessed by immediately measuring the tail current amplitudes when depolarizing cells ranging from -150 to +20 mV, after hyperpolarizing the same cells to -150 mV (**Figure 3F**). When the voltage pulse deviated the equilibrium potential of I_f, the voltage-gated channel has not yet closed and currents instantaneously reverse the flowing direction. The Tbx18-EYFP-c-kit+ cMSCs elicited typical voltage dependence I_f currents (**Figure 3G**). Linear regression, which calculated the average reversal potential, showed that Tbx18-c-kit+ cMSCs have a more positive potential compared with SAN cells (-18.41±1.2 mV, n = 12 vs. -23.19±1.6 mV, n = 10; P < 0.05) (**Figure 3H**). We further studied the activation and deactivation time constants of I_f in Tbx18-EYFP-c-kit+ cMSCs. Fitting current traces to a monoexponential function, we observed that the activation time constant ranged from 660±27 ms at -120 mV to 1880±103 ms at -80 mV, and the deactivation time constant was 1000±99 ms at -70 mV to 210±19 ms at -40 mV (**Figure 3I**). We also evaluated the effects of β-adrenergic stimulation on I_f current activation, which simulated the acute sympathetic nerve activity in Tbx18-c-kit+ cMSCs (**Figure 3J**). Given 3-μmol/L isoproterenol, the average activation time of I_f (upon steps to -120 mV) decreased by 26±2% (n = 8). Additionally, the $V_{1/2}$ was shifted approximately 6.1 mV (from -84.9±5.6 to -78.8±4.8 mV, n = 8; P < 0.05) toward the direction of depolarization. The data from both experiments showed that I_f activation was remarkably accelerated after administration. However, the slope was not notably varied (from -7.6±0.4 to -7.7±0.3 mV, n = 8; P = 0.862) (**Figure 3K**).

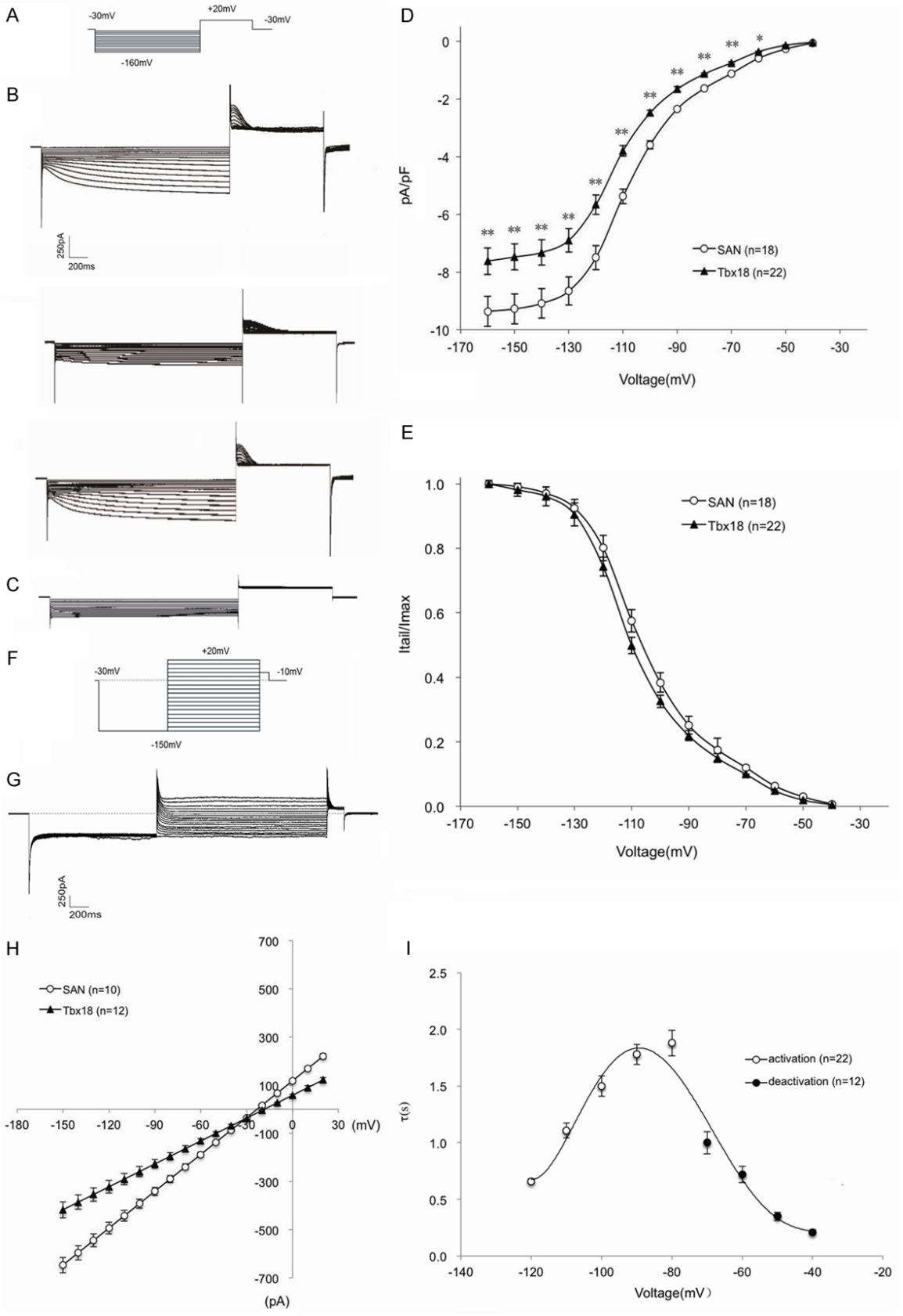
A
-30mV
+20mV
-30mV
-160mV
B
250pA
200ms
C
D
pA/pF
SAN (n=18)
Tbx18 (n=22)
Voltage(mV)
E
Itail/Imax
SAN (n=18)
Tbx18 (n=22)
Voltage(mV)
F
+20mV
-30mV
-10mV
-150mV
G
250pA
200ms
H
SAN (n=10)
Tbx18 (n=12)
(mV)
(pA)
I
τ(s)
activation (n=22)
deactivation (n=12)
Voltage(mV)

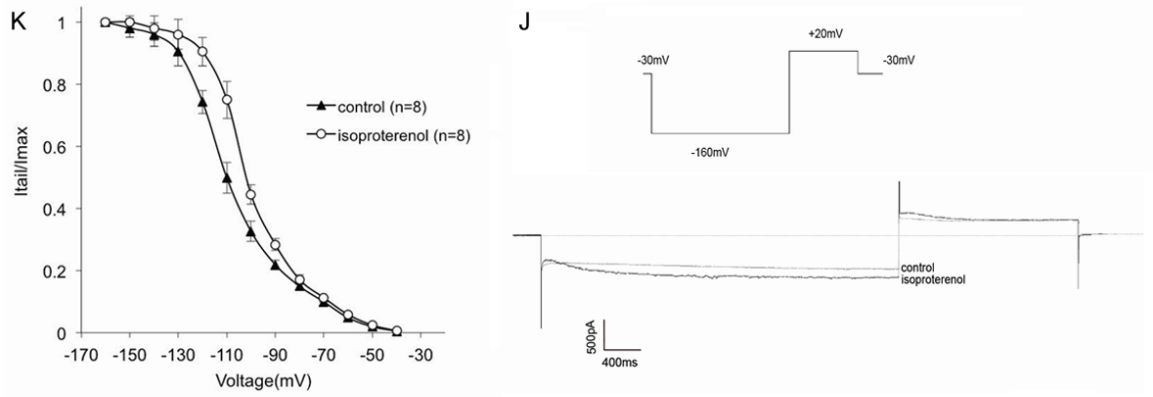

Figure 3. Functional expression of I_f in Tbx18-EYFP-c-kit+ cMSCs. (A) Voltage pulse protocol to elicit currents and evaluate activation properties of I_f. (B) Representative I_f traces (top-to-bottom) recorded from a Tbx18-EYFP-c-kit+ cMSC before, during and after 5 mmol/l Cs^+. (C) EYFP-c-kit+ cMSCs did not record any currents. (D) Current voltage (I-V) relationship of I_f in Tbx18-EYFP-c-kit+ cMSCs and canine SAN cells. Data are presented as the means ± SEM. *P < 0.05 vs. SAN; **P < 0.01 vs. SAN. (E) Normalized tail currents of Tbx18-EYFP-c-kit+ cMSCs, which were compared with SAN cells used to construct the I_f activation curves. Solid lines are the Boltzmann equation fit to the data. Data are presented as the means ± SEM. (F) Voltage pulse protocol to measure deactivation properties of I_f. (G) Typical tail current traces of I_f in Tbx18-EYFP-c-kit+ cMSCs. (H) I-V relationships of the fully activated I_f in Tbx18-EYFP-c-kit+ cMSCs and SAN cells. Solid lines are the linear fit to the different current traces under corresponding test voltage. Data are presented as the means ± SEM. (I) Time constants of (de)activation in Tbx18-EYFP-c-kit+ cMSCs. Solid line is currents elicited from activation (A) and deactivation (F) voltage pulse protocols, fit to the equation $\tau = 1/[A1 \times \exp(-V/B1) + A2 \times \exp(V/B2)]$, where τ is the activation or deactivation time constant, and A1, A2, B1, and B2 are evaluated fitting parameters [58]. (J, K) Effects of isoproterenol on the activation of I_f in Tbx18-EYFP-c-kit+ cMSCs. (J) Characteristic I_f traces elicited by a step pulse to -160 mV from holding potential of -30 mV, followed by a step to +20 mV in the absence and presence of 3 μmol/L isoproterenol (ISO). (K) Shifts of I_f activation by isoproterenol. Data arepresented as the means ± SEM.

Tbx18 overexpression in c-kit+ cMSCs upregulates SAN markers expression

The unique characteristic of cardiac pacemaker cells is the expression of hyperpolarization-activated cyclic nucleotide-gated channels (HCN channels), "funny channels" (I_f), which play critical roles with respect to the spontaneous 4 phase diastolic depolarization and the initiation of the normal heartbeat [28]. In the present study, Tbx18 overexpression led to a 12-fold increase in HCN4 protein levels in c-kit+ cMSCs (n = 3, **Figure 4C**). The difference of HCN4 protein levels between Tbx18-c-kit+ cMSCs and SAN cells did not reach statistical significance (n = 3, P = 0.056, **Figure 4C**). Inward rectifier K^+ channel (Kir2.1) is responsible for the maximum diastolic potential of slow-reaction automatism frequency cells; thus, our research demonstrated that Kir2.1 mRNA was downregulated in Tbx18-c-kit+ cMSCs compared with EYFP-c-kit+ cMSCs, and the difference was statistically significant (n = 3; P < 0.01, **Figure 4B**). Although the difference was observed between Tbx18-c-kit+ cMSCs and SAN cells (n = 3; P < 0.05, **Figure 4B**), Tbx18-c-kit+ cMSCs differentiated toward SAN cells. Additionally, the native pacemaker current exhibits autonomic responsiveness to both adrenergic and cholinergic agonists. Electrophysiological tests of native SAN channels and cloned channels demonstrated that acetylcholine and catecholamines shift the I_f activation curve toward negative and positive directions along the voltage axis [29, 30], and the negative phenomenon is due to the inhibition of adenylate cyclase, while the positive phenomenon primarily results from the direct binding of cyclic AMP (cAMP) with the HCN channel protein (CNBD) [31]. Increased levels of cAMP can activate both the I_f channel and the cAMP-dependent protein kinase A system (PKA)-mediated phosphorylation of phospholamban (PLB), which enhances the activation kinetics of intracellular and cell-surface proteins, resulting in generating robust rhythmic action potentials [32].

The present study showed that the intracellular cAMP level of Tbx18-c-kit+ cMSCs was remarkably higher than that of EYFP-c-kit+ cMSCs, reproducing the higher intracellular cAMP level exhibited in SAN cells (n = 3; P < 0.01, **Figure**

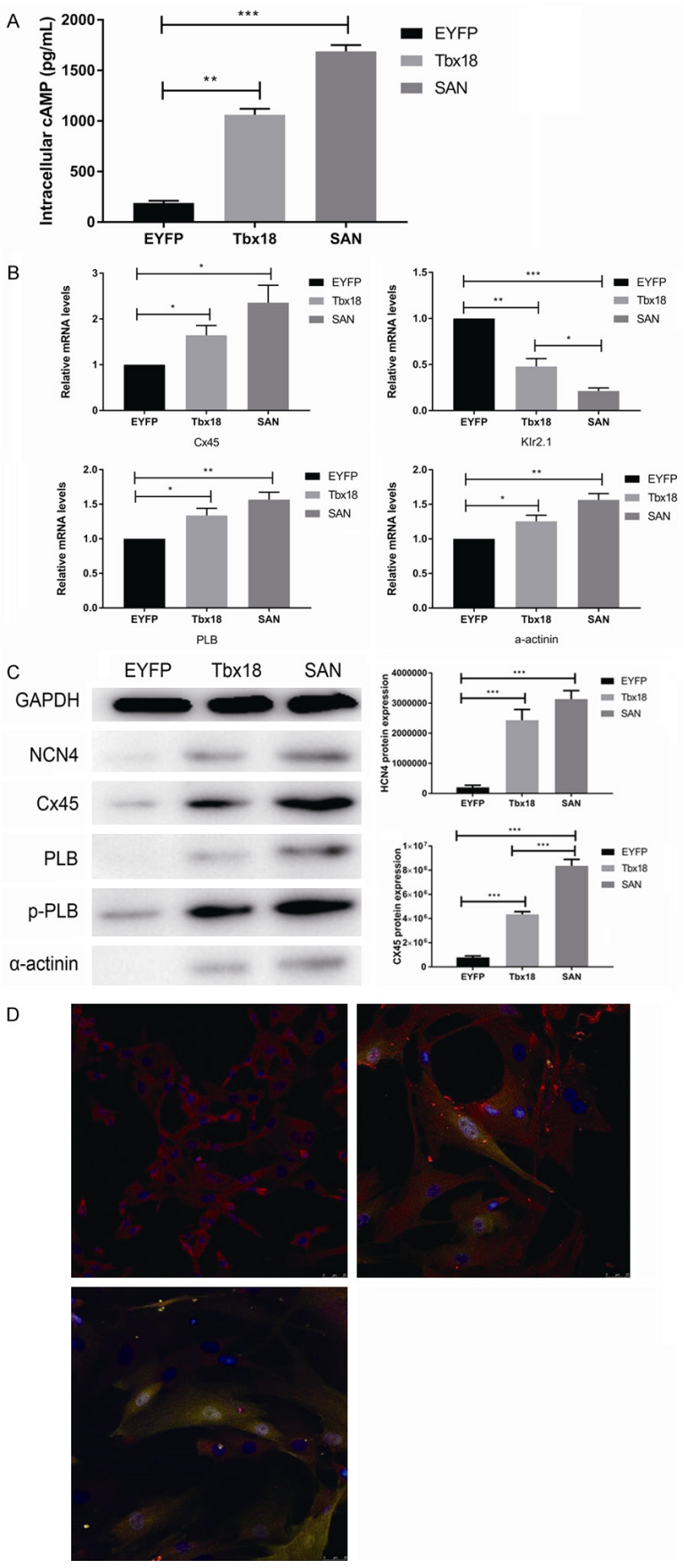

Figure 4. Tbx18-c-kit+ cMSCs recapitulate the critical features of genuine SAN pacemakers. A. Intracellular cAMP level of Tbx18–c-kit+ cMSCs was significantly higher compared to EYFP–c-kit+ cMSCs (n = 3), reproducing the higher intracellular cAMP level observed in SAN cells (n = 3). Data are presented as the means ± SEM. **P < 0.01 vs. EYFP--c-kit+ cMSCs; ***P < 0.001 vs. EYFP–c-kit+ cMSCs. B. Relative mRNA levels of Cx45, Kir2.1, PLB, α-actinin comparing Tbx18--c-kit+ cMSCs and SAN cells normalized to EYFP–c-kit+ cMSCs, respectively. Tbx18–c-kit+ cMSCs show similar pattern of normalized transcript levels of SAN cells. Similar results were obtained in 3 independent experiments, each experiment was performed with cells isolated from ≥ 3 wells from a 6-well plate. Data are presented as the means ± SEM. *P < 0.05 vs. EYFP–c-kit+ cMSCs or SAN cells; **P < 0.01 vs. EYFP–c-kit+ cMSCs; ***P < 0.001 vs. EYFP–c-kit+ cMSCs. C. HCN4, Cx45, PLB, p-PLB, α-actinin protein expression levels were detected by using western blot analysis. Similar results were obtained in 3 independent experiments, and each experiment was performed with cells isolated from the 6 wells of a 6-well plate. Data are presented as the means ± SEM. ***P < 0.001 vs. EYFP–c-kit+ cMSCs or SAN cells. D. Cx45 immunofluorescence image (Cx45-red, nuclei-blue) of SAN cells (upper, left), Tbx18-c-kit+ cMSCs (upper, right) and EYFP–c-kit+ cMSCs (bottom). Scale bar: 25 μm.

4A). This result is consistent with the findings of Vinogradova [33]. We also evaluated the special features of cardiac myocytes in Tbx18-c-kit+ cMSCs: PLB combined with the sarcoplasmic reticulum Ca^{2+} ATPase (SERCA) inhibits the pumping of free calcium into the sarcoplasmic reticulum in a non-phosphorylation state; phosphorylation of phospholamban (p-PLB), phosphorylation state of phos-

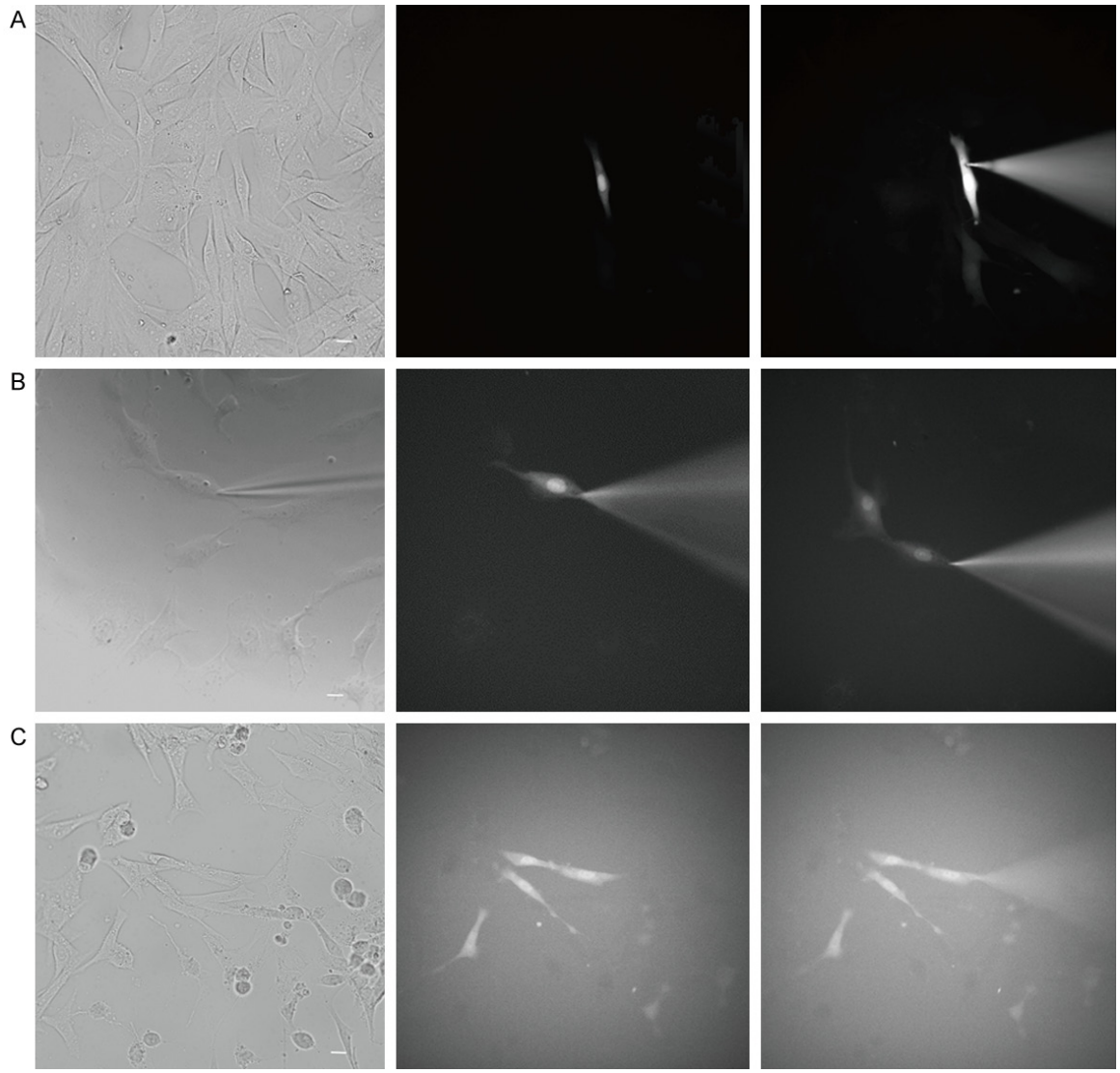

Figure 5. Dye diffused into neighboring atrial cells. (A) The 0.1% Lucifer yellow dye was loaded into Tbx18-EYFP–c-kit$^+$ cMSCs (fluorescent cell, I_f currents expression, n = 6), (B) a SAN cell (I_f currents expression, n = 3) and (C) an EYFP–c-kit$^+$ cMSC (fluorescent cell, n = 6) respectively. After the 5-min dye transfer, (A) two adjacent atrial cells are displayed, (B) one adjacent cell was displayed, and (C) the dye did not diffuse into any adjacent atrial cells. Scale bar = 20 μm.

pholamban; α-actinin, a microfilament protein found in skeletal muscle cells and smooth muscle cells. The present results showed that the overexpression of Tbx18 significantly increased the expression of PLB, p-PLB and α-actinin at the mRNA and protein levels (n = 3; $P < 0.05$, **Figure 4B**, **4C**) and the changes toward SAN cells. Electrical propagation in the heart is mediated by gap junctions, aggregates of transmembrane channels composed of connexins [34]. Twenty-one connexins in the human genome have been identified so far, four of which, connexin 43 (Cx43), Cx40, Cx45 and Cx37, are differently expressed in cardiac tissues and transfer distinctive passive electrical signals to different regions of the heart [35]. Cx45 is preferentially expressed in SAN cells and can assemble gap junction channels with low conduction [34]. The present study demonstrated that Cx45 mRNA was upregulated in Tbx18-c-kit$^+$ cMSCs compared with that in EYFP-c-kit$^+$ cMSCs, and this difference was statistically significant (n = 3; $P < 0.05$, **Figure 4B**). In protein expression, Tbx18-c-kit$^+$ cMSCs resembled native SAN cells, which had strong positive Cx45 expression and led to a 5.6-fold increase of

Cx45 compared to EYFP-c-kit+ cMSCs (n = 3, **Figure 4C**, **4D** upper right).

Gap-junctional intercellular communication under co-culture conditions

We further investigated whether Tbx18-EYFP-c-kit+ cMSCs had established gap-junctional coupling with the neighboring atrial cells by using the dye transfer method. The target cell was identified through fluorescent in the dark field and expressing I_f currents (Tbx18-EYFP-c-kit+ cMSC) or fluorescent in the dark field (EYFP-c-kit+ cMSC). After 5 minutes of dye diffusion, two neighboring atrial cells of a Tbx18-EYFP-c-kit+ cMSCs were also fluorescent (**Figure 5A**), whereas no neighboring atrial cells of EYFP-c-kit+ cMSCs were fluorescent (**Figure 5C**). A SAN cell was identified by configuration. The internal solution containing 0.1% Lucifer yellow dye was loaded to make one SAN cell of the pair fluorescent. After 5 minutes of dye diffusion, the other cell of this pair was also fluorescent (**Figure 5B**).

Discussion

The present study successfully induced c-kit+ cMSCs differentiation into SAN-like pacemaker cells by overexpressing the transcription factor Tbx18, which represses working myocardium gene expression and initiates the SAN program. Unlike EYFP-c-kit+ cMSCs, Tbx18-c-kit+ cMSCs have similar major distinctive characteristics of native canine SAN cells with respect to electrophysiological properties and gap connexin expression profiles. When co-cultured with canine atrial cells, Tbx18-c-kit+ cMSCs recorded functional I_f currents and formed dye coupling with adjacent atrial cells.

An ideal biological pacemaker not only possess robust and sustained automaticity, but can also integrate with neighboring atrial cells to construct an effective syncytium. Cardiomyocyte and vasculature regeneration depend on the function of the c-kit receptor, which is expressed on bone marrow stemcells and are identified as cardiac stem cell [14, 36]. The pro-angiogenic milieu may facilitate the function of the pacemaker, and c-kit+ cMSCs are a heart-specific MSC population with cardiovascular commitment potential, which is why we adopted c-kit+ cMSCs in favor of cMSCs. During cardiogenesis, a complicated net of transcriptional factors regulates the primitive myocytes specialized to ventricular, atrial, and pacemaker fates. Upstream of these factors is Tbx18, which induces SAN-specific conversion [17, 37]. The Tbx18 protein has a conserved DNA-binding region and a conserved interaction domain for other transcription factors [38]. An elegant study showed that only a single Tbx18 suffices for the direct conversion of quiescent cardiomyocytes to pacemaker cells without additional cytokines [39]. In the present study, c-kit+-cMSCs were first sorted and then transfected with lentiviral pLV-hTbx18-yellow fluorescent protein; c-kit+-cMSCs transfected with lentiviral pLV-yellow fluorescent protein served as a control group. At 48 h after transfection, yellow fluorescent expression was observed in > 90% of both infected cells. Additionally, RT-PCR verified the TBX18 gene expression in Tbx18-EYFP-c-kit+ cMSCs. For better comparison between Tbx18-EYFP-c-kit+ cMSCs and native SAN cells, we isolated and cultured canine SAN cells simultaneously as a positive control group.

At 4 days after transfection, we selected several critical features of SAN cells to compare the differences among Tbx18-c-kit+-cMSCs, c-kit+-cMSCs and SAN cells at the mRNA and protein levels. The difference of relative mRNA level of Kir2.1 between Tbx18-c-kit+ cMSCs and SAN cells was significant. Compared solely with YFP-transfected c-kit+-cMSCs, both Tbx18-transfected c-kit+-cMSCs and canine SAN cells have significantly lower relative mRNA levels of Kir2.1. Tbx18-transfected c-kit+-cMSCs have less I_{k1} channels, and bear smaller negative values of maximum diastolic potential compared with EYFP-c-kit+ cMSCs. In the heart, I_{K1} plays a critical role in maintaining resting potential and determining the shape of the terminal phase of repolarization, which governs the automaticity of the pacemaker. The down-regulation of hyperpolarizing current I_{K1} was one approach to build a gene-based biological pacemaker. Miake and colleagues converted a quiescent ventricular preparation to a spontaneous depolarization biological pacemaker through reducing the outward current I_{K1}. These authors were the first to use an ion channel method and the isolated Kir2.1-suppressed transduced cells, showing 4-phase spontaneous depolarization. However, the major problem of this strategy was the prolongation of the QT interval showing

that the modification of the ion channel was not the best target [40]. The faithful recapitulation of the sophisticated pacemaker is more complicated. A further special feature of SAN cells is the expression of hyperpolarization-activated cyclic nucleotide-gated channels (HCN channels), "funny channels" (I_f), which is one type of inward current important for the membrane potential depolarization of SAN cells. Four members of the hyperpolarization-activated cyclic nucleotide-gated gene (HCN1-4) family encode funny channels, which have different features in activation kinetics and cAMP sensitivities. The isoform HCN4 is most widely present in the SAN of lower mammals and humans, and HCN1 and HCN2 can also be detected, but at extremely low levels in different species. SAN cannot detect HCN3 [22, 41-44]. HCN4 knockout mice and human HCN4 mutations showed that HCN4 is indispensable during heart formation and is also important for pacemaker rhythm maintenance [22, 45-48]. In the present study, HCN4 protein expression was detected in Tbx18-c-kit+ cMSCs, and the difference of HCN4 protein expression between Tbx18-c-kit+ cMSCs and SAN cells did not reach statistical significance ($P = 0.056$, $n = 3$). The voltage amplitude and second messenger pathway collaboratively manage the opening of HCN channels. Molecular studies have revealed the presence of a cyclic nucleotide-binding domain (CNBD) in the C-terminal of the HCN gene family. The cAMP binding HCN channel directly controlled channel function [49]. The present study found that the intracellular cAMP level of Tbx18-c-kit+ cMSCs was notably higher than that of EYFP-c-kit+ cMSCs, and increased β-adrenergic stimulation shifted the activation curve of I_f currents in Tbx18-c-kit+ cMSCs towards positive direction along the voltage axis, showing the autonomic agonists responsiveness. The α-actinin mRNA expression was upregulated, and protein expression was detected in Tbx18-c-kit+ cMSCs displaying cardiac myocyte differentiation potential. PLB is a transmembrane protein located on the sarcoplasmic reticulum of cardiac myocytes. This protein is phosphorylated, and p-PLB relieves the inhibition effect on sarcoplasmic reticulum Ca^{2+}-ATPase (SERCA), thereby facilitating the reuptake of Ca^{2+} by internal stores [50]. PLB mRNA expression was upregulated, and protein expression was detected in Tbx18-c-kit+ cMSCs. Interestingly, we found that the p-PLB protein expression in Tbx18-c-kit+ cMSCs was higher than the PLB protein expression. We speculated that the elevated cAMP level reflected the lower association between SERCA and PLB through the phosphorylation of PLB by PKA. Another critical feature of SAN cells is the expression of Cx45 protein, and gap junctions can form communication channels between adjacent cells to enable the intercellular transfer of ions, small molecules and electrical impulses. Although there was a difference in the Cx45 protein expression between Tbx18-c-kit+ cMSCs and SAN cells, the protein level was 5.6-fold higher than that in EYFP-c-kit+ cMSCs.

Under co-culture conditions, we evaluated the characteristics of typical I_f elicited in Tbx18-c-kit+ cMSCs compared with that of SAN cells. In the dark field, Tbx18-c-kit+ cMSCs and EYFP-c-kit+ cMSCs can be easily identified and examined by using the whole-cell patch clamp technique. We tested the activation and deactivation properties of I_f currents recorded in Tbx18-c-kit+ cMSCs under different voltage protocols. The I_f density of Tbx18-c-kit+ cMSCs and canine SAN cells was alike and represented the characteristic of I_f obtained in large animals. Regression models demonstrated the trend of I_f currents in Tbx18-c-kit+ cMSCs and canine SAN cells was highly similar. Compared with native canine SAN cells, the $V_{1/2}$ of Tbx18-c-kit+ cMSCs was more negative and the average reversal potential was more positive. Applying sympathomimetic amines, the activation curve of Tbx18-c-kit+ cMSCs was shifted right along the voltage axis and the activation time was shortened accordingly. Previous studies have shown that the reproduction of the precise native kinetic and modulatory properties of native I_f channels failed by the heterologous expression of HCN isoforms. HCN4 heteromers can generate I_f currents approaching those of native SAN I_f channels, but these currents do not display identical voltage dependence on activation properties [51]. The $V_{1/2}$ of same HCN isoform was -76 mV and -96 mV in neonatal and adult ventricle myocytes, respectively, and this difference was not small [24].

In the present study, we showed that endogenous I_f channels generated from induced Tbx18-c-kit+ cMSCs have similar current densities and β-adrenergic stimulation responsiveness to SAN cells, but do not have precisely the

same properties. We thought this difference resulted from two aspects: 1) additional modulatory elements, such as protein-protein and protein-phospholipid interactions, along with modulatory cytoplasmic factors that modulate I_f current. Thus, context dependence is important [52]. 2) The I_f channel is not a mature channel; it is in the early stage of differentiation. Although the current density is smaller and the reversal potential is more positive, this I_f channel has almost the complete features of native canine I_f channels. We further assessed gap-junctional coupling between Tbx18-c-kit+ cMSCs and atrial cells by using the dye transfer method. Gap junction channels consist of two hemichannels (connexons) oligomerized from connexin (Cx) proteins, which are formed by 21 distinct isoforms. The formation patterns have homotypic (same Cx isotype in both hemichannels), heterotypic (hemichannels differ in Cx isotypes) and heteromeric (different Cx isotypes in at least one hemichannel) channels. Experimental evidence shows that three connexins, Cx40, Cx43 and Cx45, are expressed in the myocytes of distinct regions of the heart tissue. Cx43 is abundantly expressed in atria and ventricles, while Cx45 is mostly restricted to SAN cells. Heterotypic Cx43/Cx45 are responsible for the action potential propagation from the SAN cells to atrial myocytes, while Cx40 cannot form functional heterotypic gap junction channels with Cx45 [34, 53]. In the present study, by using SAN cells expressing homotypic channels with Cx45, and Tbx18-c-kit+ cMSCs in co-culture with atrial cells expressing heterotypic channels with Cx43/Cx45, we counted the number of fluorescent cells dye loaded into the target cells after 5 minutes. Although different connexin channels have different permeabilities, Lucifer yellow passes through all connexin channels [54]. Thus, we compared the permeability of gap junctions comprised of different connexins by using Lucifer yellow. The critical electrical cell-cell coupling between heterologous cell pairs was observed within 24 to 36 h, enabling this pair to function as a pacemaker unit [55]. These data were obtained after 3 days under co-culture conditions. No neighboring atrial cell of an EYFP-c-kit+ cMSC was fluorescent, indicating that no or few gap junction channels were formed. Gap junction coupling conductance (G_j) is quantitatively determined by three factors: $G_j = N \times \gamma_j \times P_{open}$, the number of functional gap junction channels (N), the unitary channel conductance (γ_j) and the gap junction channel open probability (P_{open}). V_j-gating is a general feature for all characterized gap junction channels. Previous studies have shown that the γ_j of Cx45 gap junctions is lower than those formed by Cx40 or Cx43, and Cx43/Cx45 gap junction channels have faster V_j-gating kinetics than Cx45/Cx45 gap junction channels [56, 57]. The present study showed that more adjacent cells of Tbx18-c-kit+ cMSCs were fluorescent than those of SAN cells after 5 minutes of dye diffusion under co-culture conditions, consistent with the findings of the previous experiments. In conclusion, we expressed a gene critical for early SAN specification in c-kit+ cMSCs to construct faithful biological replicas of rare SAN cells. The results showed that c-kit+ cMSCs were effectively transfected by a lentiviral vector encoding a human Tbx18 (hTbx18) gene and a yellow fluorescent protein (YFP) gene, and these c-kit+ cMSCs were capable of expressing hTbx18. The overexpression of Tbx18 in c-kit+ cMSCs could generate functional I_f currents, sensitively respond to autonomicnerve modulations and obtain other epigenetic features of SAN cells. Under co-culture conditions, Tbx18-c-kit+ cMSC can form functional gap junction channels with atrial cells. To our knowledge, the present study is the first report describing hTbx18 transfected c-kit+-cMSCs co-cultured with canine atrial cells to examine their differentiation fate compared with that of canine SAN cells. These findings lay the groundwork for future studies investigating cell-based biological pacemakers in vivo.

Acknowledgements

This study was supported by the National Natural Science Foundation of China (NO. 8157-0300).

Disclosure of conflict of interest

None.

Address correspondence to: Drs. Shu Lin and Zhi-Yuan Song, Department of Cardiology, Southwest Hospital, The Third Military Medical University, 30 Gaotanyan Road, Shapingba, Chongqing 400038, P.R. China. Tel: 86 15683713870; E-mail: shulin1956@126.com (SL); Tel: 86 13908327066; E-mail: zysong2010@126.com (ZYS)

References

[1] Chauveau S, Brink PR and Cohen IS. Stem cell-based biological pacemakers from proof of principle to therapy: a review. Cytotherapy 2014; 16: 873-880.

[2] Valiunas V, Doronin S, Valiuniene L, Potapova I, Zuckerman J, Walcott B, Robinson RB, Rosen MR, Brink PR and Cohen IS. Human mesenchymal stem cells make cardiac connexins and form functional gap junctions. J Physiol 2004; 555: 617-626.

[3] Xu M, Wani M, Dai YS, Wang J, Yan M, Ayub A and Ashraf M. Differentiation of bone marrow stromal cells into the cardiac phenotype requires intercellular communication with myocytes. Circulation 2004; 110: 2658-2665.

[4] Hatzistergos KE, Quevedo H, Oskouei BN, Hu Q, Feigenbaum GS, Margitich IS, Mazhari R, Boyle AJ, Zambrano JP, Rodriguez JE, Dulce R, Pattany PM, Valdes D, Revilla C, Heldman AW, McNiece I and Hare JM. Bone marrow mesenchymal stem cells stimulate cardiac stem cell proliferation and differentiation. Circ Res 2010; 107: 913-922.

[5] Makino S, Fukuda K, Miyoshi S, Konishi F, Kodama H, Pan J, Sano M, Takahashi T, Hori S, Abe H, Hata J, Umezawa A and Ogawa S. Cardiomyocytes can be generated from marrow stromal cells in vitro. J Clin Invest 1999; 103: 697-705.

[6] Morishita Y and Taira A. Sino-atrial node transplantation: an experimental study. Rinsho Kyobu Geka 1983; 3: 18-22.

[7] Zhang H, Lau DH, Shlapakova IN, Zhao X, Danilo P, Robinson RB, Cohen IS, Qu D, Xu Z and Rosen MR. Implantation of sinoatrial node cells into canine right ventricle: biological pacing appears limited by the substrate. Cell Transplant 2011; 20: 1907-1914.

[8] Jun C, Zhihui Z, Lu W, Yaoming N, Lei W, Yao Q and Zhiyuan S. Canine bone marrow mesenchymal stromal cells with lentiviral mHCN4 gene transfer create cardiac pacemakers. Cytotherapy 2012; 14: 529-539.

[9] Nong Y, Zhang C, Wei L, Zhang Z, Cheng J, Wen L and Song Z. In situ investigation of allografted mouse HCN4 gene-transfected rat bone marrow mesenchymal stromal cells with the use of patch-clamp recording of ventricular slices. Cytotherapy 2013; 15: 905-919.

[10] Feng Y, Luo S, Tong S, Zhong L, Zhang C, Yang P and Song Z. Electric-pulse current stimulation increases if current in mShox2 genetically modified canine mesenchymal stem cells. Cardiology 2015; 132: 49-57.

[11] Orlic D, Kajstura J, Chimenti S, Jakoniuk I, Anderson SM, Li B, Pickel J, McKay R, Nadal-Ginard B, Bodine DM, Leri A and Anversa P. Bone marrow cells regenerate infarcted myocardium. Nature 2001; 410: 701-705.

[12] Czarna A, Sanada F, Matsuda A, Kim J, Signore S, Pereira JD, Sorrentino A, Kannappan R, Cannata A, Hosoda T, Rota M, Crea F, Anversa P and Leri A. Single-cell analysis of the fate of c-kit-positive bone marrow cells. NPJ Regen Med 2017; 2: 27.

[13] Beltrami AP, Barlucchi L, Torella D, Baker M, Limana F, Chimenti S, Kasahara H, Rota M, Musso E, Urbanek K, Leri A, Kajstura J, Nadal-Ginard B and Anversa P. Adult cardiac stem cells are multipotent and support myocardial regeneration. Cell 2003; 114: 763-776.

[14] Pagliari S, Jelinek J, Grassi G and Forte G. Targeting pleiotropic signaling pathways to control adult cardiac stem cell fate and function. Front Physiol 2014; 5: 219.

[15] Christoffels VM, Smits GJ, Kispert A and Moorman AF. Development of the pacemaker tissues of the heart. Circ Res 2010; 106: 240-254.

[16] Christoffels VM, Mommersteeg MT, Trowe MO, Prall OW, de Gier-de Vries C, Soufan AT, Bussen M, Schuster-Gossler K, Harvey RP, Moorman AF and Kispert A. Formation of the venous pole of the heart from an Nkx2-5-negative precursor population requires Tbx18. Circ Res 2006; 98: 1555-1563.

[17] Wiese C, Grieskamp T, Airik R, Mommersteeg MT, Gardiwal A, de Gier-de Vries C, Schuster-Gossler K, Moorman AF, Kispert A and Christoffels VM. Formation of the sinus node head and differentiation of sinus node myocardium are independently regulated by Tbx18 and Tbx3. Circ Res 2009; 104: 388-397.

[18] Feng Y, Yang P, Luo S, Zhang Z, Li H, Zhu P and Song Z. Shox2 influences mesenchymal stem cell fate in a co-culture model in vitro. Mol Med Rep 2016; 14: 637-642.

[19] Kim MO, Jung H, Kim SC, Park JK and Seo YK. Electromagnetic fields and nanomagnetic particles increase the osteogenic differentiation of human bone marrow-derived mesenchymal stem cells. Int J Mol Med 2015; 35: 153-160.

[20] Wu Y, Gao Z, Chen B, Koval OM, Singh MV, Guan X, Hund TJ, Kutschke W, Sarma S, Grumbach IM, Wehrens XH, Mohler PJ, Song LS and Anderson ME. Calmodulin kinase II is required for fight or flight sinoatrial node physiology. Proc Natl Acad Sci U S A 2009; 106: 5972-5977.

[21] Yeh YH, Burstein B, Qi XY, Sakabe M, Chartier D, Comtois P, Wang Z, Kuo CT and Nattel S. Funny current downregulation and sinus node dysfunction associated with atrial tachyarrhythmia: a molecular basis for tachycardia-bradycardia syndrome. Circulation 2009; 119: 1576-1585.

[22] Moosmang S, Stieber J, Zong X, Biel M, Hofmann F and Ludwig A. Cellular expression and functional characterization of four hyperpolarization-activated pacemaker channels in cardiac and neuronal tissues. Eur J Biochem 2001; 268: 1646-1652.
[23] Yasui K, Liu W, Opthof T, Kada K, Lee JK, Kamiya K and Kodama I. I(f) current and spontaneous activity in mouse embryonic ventricular myocytes. Circ Res 2001; 88: 536-542.
[24] Qu J, Barbuti A, Protas L, Santoro B, Cohen IS and Robinson RB. HCN2 overexpression in newborn and adult ventricular myocytes: distinct effects on gating and excitability. Circ Res 2001; 89: E8-14.
[25] Wilders R, Verheijck EE, Kumar R, Goolsby WN, van Ginneken AC, Joyner RW and Jongsma HJ. Model clamp and its application to synchronization of rabbit sinoatrial node cells. Am J Physiol 1996; 271: H2168-2182.
[26] Mangoni ME and Nargeot J. Properties of the hyperpolarization-activated current (I(f)) in isolated mouse sino-atrial cells. Cardiovasc Res 2001; 52: 51-64.
[27] Verkerk AO, Wilders R, van Borren MM, Peters RJ, Broekhuis E, Lam K, Coronel R, de Bakker JM and Tan HL. Pacemaker current (I(f)) in the human sinoatrial node. Eur Heart J 2007; 28: 2472-2478.
[28] Biel M, Schneider A and Wahl C. Cardiac HCN channels: structure, function, and modulation. Trends Cardiovasc Med 2002; 12: 206-212.
[29] Ludwig A, Zong X, Jeglitsch M, Hofmann F and Biel M. A family of hyperpolarization-activated mammalian cation channels. Nature 1998; 393: 587-591.
[30] Santoro B, Liu DT, Yao H, Bartsch D, Kandel ER, Siegelbaum SA and Tibbs GR. Identification of a gene encoding a hyperpolarization-activated pacemaker channel of brain. Cell 1998; 93: 717-729.
[31] DiFrancesco D and Tortora P. Direct activation of cardiac pacemaker channels by intracellular cyclic AMP. Nature 1991; 351: 145-147.
[32] Lakatta EG and Maltsev VA. Reprogramming paces the heart. Nat Biotechnol 2013; 31: 31-32.
[33] Vinogradova TM, Lyashkov AE, Zhu W, Ruknudin AM, Sirenko S, Yang D, Deo S, Barlow M, Johnson S, Caffrey JL, Zhou YY, Xiao RP, Cheng H, Stern MD, Maltsev VA and Lakatta EG. High basal protein kinase A-dependent phosphorylation drives rhythmic internal Ca2+ store oscillations and spontaneous beating of cardiac pacemaker cells. Circ Res 2006; 98: 505-514.
[34] Vozzi C, Dupont E, Coppen SR, Yeh HI and Severs NJ. Chamber-related differences in connexin expression in the human heart. J Mol Cell Cardiol 1999; 31: 991-1003.
[35] Kwong KF, Schuessler RB, Green KG, Laing JG, Beyer EC, Boineau JP and Saffitz JE. Differential expression of gap junction proteins in the canine sinus node. Circ Res 1998; 82: 604-612.
[36] Fazel S, Cimini M, Chen L, Li S, Angoulvant D, Fedak P, Verma S, Weisel RD, Keating A and Li RK. Cardioprotective c-kit+ cells are from the bone marrow and regulate the myocardial balance of angiogenic cytokines. J Clin Invest 2006; 116: 1865-1877.
[37] Szabo E, Rampalli S, Risueno RM, Schnerch A, Mitchell R, Fiebig-Comyn A, Levadoux-Martin M and Bhatia M. Direct conversion of human fibroblasts to multilineage blood progenitors. Nature 2010; 468: 521-526.
[38] Tada M and Smith JC. T-targets: clues to understanding the functions of T-box proteins. Dev Growth Differ 2001; 43: 1-11.
[39] Kapoor N, Liang W, Marban E and Cho HC. Direct conversion of quiescent cardiomyocytes to pacemaker cells by expression of Tbx18. Nat Biotechnol 2013; 31: 54-62.
[40] Miake J, Marban E and Nuss HB. Functional role of inward rectifier current in heart probed by Kir2.1 overexpression and dominant-negative suppression. J Clin Invest 2003; 111: 1529-1536.
[41] Liu J, Dobrzynski H, Yanni J, Boyett MR and Lei M. Organisation of the mouse sinoatrial node: structure and expression of HCN channels. Cardiovasc Res 2007; 73: 729-738.
[42] Tellez JO, Dobrzynski H, Greener ID, Graham GM, Laing E, Honjo H, Hubbard SJ, Boyett MR and Billeter R. Differential expression of ion channel transcripts in atrial muscle and sinoatrial node in rabbit. Circ Res 2006; 99: 1384-1393.
[43] Brioschi C, Micheloni S, Tellez JO, Pisoni G, Longhi R, Moroni P, Billeter R, Barbuti A, Dobrzynski H, Boyett MR, DiFrancesco D and Baruscotti M. Distribution of the pacemaker HCN4 channel mRNA and protein in the rabbit sinoatrial node. J Mol Cell Cardiol 2009; 47: 221-227.
[44] Chandler NJ, Greener ID, Tellez JO, Inada S, Musa H, Molenaar P, Difrancesco D, Baruscotti M, Longhi R, Anderson RH, Billeter R, Sharma V, Sigg DC, Boyett MR and Dobrzynski H. Molecular architecture of the human sinus node: insights into the function of the cardiac pacemaker. Circulation 2009; 119: 1562-1575.
[45] Herrmann S, Stieber J and Ludwig A. Pathophysiology of HCN channels. Pflugers Arch 2007; 454: 517-522.
[46] Stieber J, Herrmann S, Feil S, Loster J, Feil R, Biel M, Hofmann F and Ludwig A. The hyperpolarization-activated channel HCN4 is required for the generation of pacemaker action poten-

tials in the embryonic heart. Proc Natl Acad Sci U S A 2003; 100: 15235-15240.
[47] Herrmann S, Stieber J, Stockl G, Hofmann F and Ludwig A. HCN4 provides a 'depolarization reserve' and is not required for heart rate acceleration in mice. EMBO J 2007; 26: 4423-4432.
[48] Maltsev VA and Lakatta EG. The funny current in the context of the coupled-clock pacemaker cell system. Heart Rhythm 2012; 9: 302-307.
[49] Robinson RB and Siegelbaum SA. Hyperpolarization-activated cation currents: from molecules to physiological function. Annu Rev Physiol 2003; 65: 453-480.
[50] MacLennan DH and Kranias EG. Phospholamban: a crucial regulator of cardiac contractility. Nat Rev Mol Cell Biol 2003; 4: 566-577.
[51] Altomare C, Terragni B, Brioschi C, Milanesi R, Pagliuca C, Viscomi C, Moroni A, Baruscotti M and DiFrancesco D. Heteromeric HCN1-HCN4 channels: a comparison with native pacemaker channels from the rabbit sinoatrial node. J Physiol 2003; 549: 347-359.
[52] Baruscotti M, Barbuti A and Bucchi A. The cardiac pacemaker current. J Mol Cell Cardiol 2010; 48: 55-64.
[53] Rackauskas M, Kreuzberg MM, Pranevicius M, Willecke K, Verselis VK and Bukauskas FF. Gating properties of heterotypic gap junction channels formed of connexins 40, 43, and 45. Biophys J 2007; 92: 1952-1965.
[54] Elfgang C, Eckert R, Lichtenberg-Frate H, Butterweck A, Traub O, Klein RA, Hulser DF and Willecke K. Specific permeability and selective formation of gap junction channels in connexin-transfected HeLa cells. J Cell Biol 1995; 129: 805-817.
[55] Valiunas V, Kanaporis G, Valiuniene L, Gordon C, Wang HZ, Li L, Robinson RB, Rosen MR, Cohen IS and Brink PR. Coupling an HCN2-expressing cell to a myocyte creates a two-cell pacing unit. J Physiol 2009; 587: 5211-5226.
[56] Ye WG, Yue B, Aoyama H, Kim NK, Cameron JA, Chen H and Bai D. Junctional delay, frequency, and direction-dependent uncoupling of human heterotypic Cx45/Cx43 gap junction channels. J Mol Cell Cardiol 2017; 111: 17-26.
[57] Palacios-Prado N and Bukauskas FF. Heterotypic gap junction channels as voltage-sensitive valves for intercellular signaling. Proc Natl Acad Sci U S A 2009; 106: 14855-14860.
[58] Qu J, Kryukova Y, Potapova IA, Doronin SV, Larsen M, Krishnamurthy G, Cohen IS and Robinson RB. MiRP1 modulates HCN2 channel expression and gating in cardiac myocytes. J Biol Chem 2004; 279: 43497-43502.